The EMBO Journal Vol. 20 No. 19 pp. 5320–5331, 2001

Crystal structure of human protein kinase CK2: insights into basic properties of the CK2 holoenzyme

Karsten Niefind[1], Barbara Guerra[2], Inessa Ermakowa and Olaf-Georg Issinger[2]

Universität zu Köln, Institut für Biochemie, Zülpicher Straße 47, D-50674 Köln, Germany and [2]Syddansk Universitet, Institut for Biokemi og Molekylær Biologi, Campusvej 55, DK-5230 Odense, Denmark

[1]Corresponding author
e-mail: Karsten.Niefind@uni-koeln.de

The crystal structure of a fully active form of human protein kinase CK2 (casein kinase 2) consisting of two C-terminally truncated catalytic and two regulatory subunits has been determined at 3.1 Å resolution (Protein Data Bank code: 1JWH). In the CK2 complex the regulatory subunits form a stable dimer linking the two catalytic subunits, which make no direct contact with one another. Each catalytic subunit interacts with both regulatory chains, predominantly via an extended C-terminal tail of the regulatory subunit. The CK2 structure is consistent with its constitutive activity and with a flexible role of the regulatory subunit as a docking partner for various protein kinases. Furthermore it shows an inter-domain mobility in the catalytic subunit known to be functionally important in protein kinases and detected here for the first time directly within one crystal structure.

Keywords: casein kinase 2/CK2 holoenzyme/constitutive activity/protein kinase CK2/X-ray crystallography

Introduction

Protein kinase CK2 (casein kinase 2) is one of the most unspecific eukaryotic protein kinases: first, >160 *in vitro* protein substrates of CK2 have been described to date (Pinna and Meggio, 1997); secondly, CK2 shows the rare ability to use either ATP or GTP as phosphoryl donor (dual-co-substrate specificity) (Niefind *et al*., 1999); thirdly, although known as a serine/threonine kinase for several decades, the capability of CK2 also to phosphorylate tyrosine has been reported repeatedly in recent years (Chardot *et al*., 1995; Wilson *et al*., 1997; Marin *et al*., 1999); and fourthly, CK2 activity was found not only with the natural cofactor Mg^{2+} but also with other divalent cations such as Mn^{2+} and Co^{2+} (Gatica *et al*., 1993).

These biochemical properties and its biomedical significance (Guerra and Issinger, 1999) make CK2 a favourite research subject. The enzyme has been found in all eukaryotic cells investigated so far and is highly conserved in evolution, indicating its critical function in cellular life. Within the phylogenetic tree of the protein kinases the catalytic core of CK2 belongs to the CMCG group (Hanks and Hunter, 1995) meaning that its nearest neighbours are key regulatory enzymes, including the cyclin-dependent kinases (CDK) or the mitogen-activated protein kinases. CK2 is essential for the viability of a cell (Padmanabha *et al*., 1990), and overexpression of its catalytic subunit is correlated with lymphoma development in transgenic mice (Seldin and Leder, 1995).

Not least due to its unspecific activity profile and its wide occurrence in tissues and cell compartments, the exact cellular functions of CK2 remain elusive. The metabolic roles of the >160 *in vitro* substrates of CK2 identified so far (Pinna and Meggio, 1997) have led to many hypotheses about the involvement of CK2 in carcinogenesis, viral tumorigenesis, transcriptional control, apoptosis, cell cycle, signal transduction and other key biological processes (Guerra and Issinger, 1999). It is generally accepted that CK2 plays an important role in cell proliferation and embryogenesis.

In parallel with its functional diversity CK2 also presents a complex picture concerning its quaternary structure. *In vivo* it exists mainly as a holoenzyme composed of two catalytic subunits (CK2α) and two regulatory subunits (CK2β). Two isoforms of the catalytic subunit (CK2α and CK2α′) have been found in human and many other sources and CK2 complexes of $\alpha_2\beta_2$, $\alpha\alpha'\beta_2$ and $\alpha'_2\beta_2$ stoichiometry can occur (Chester *et al*., 1995). Moreover there is increasing evidence that the isolated subunits can exist *in vivo* under certain circumstances and possibly have specific functions (Pinna and Meggio, 1997). *In vitro* the CK2 holoenzyme forms spontaneously from the individual subunits by a self-assembly mechanism mediated by dimerization of the two CK2β chains (Graham and Litchfield, 2000). The formation of higher oligomeric states of CK2 was also observed *in vitro* (Glover, 1986).

At the level of tertiary structure the current knowledge about CK2 is restricted to the individual subunits. Crystal structures have been published for recombinant maize CK2α (rmCK2α; Niefind *et al*., 1998) and for recombinant and C-terminally truncated human CK2β (rhCK2β^{Δ}; Chantalat *et al*., 1999), while for the CK2 holoenzyme only a theoretical model derived from the crystal structure of maize CK2α in complex with a short peptide of human CK2β exists (Battistutta *et al*., 2000). This model suggests a direct contact of the two CK2α subunits within the CK2 complex and is therefore in conflict with yeast two-hybrid system studies showing that CK2α molecules are able to bind to CK2β but not to each other (Gietz *et al*., 1995; Boldyreff *et al*., 1996).

To clarify this conflict and to rationalize some of the specific biochemical properties of the CK2 holoenzyme on a structural level we describe here for the first time the crystal structure of a complete CK2 tetramer. For this work we used recombinant human CK2. Human CK2α is normally 391 amino acids long (Figure 1A) and has a

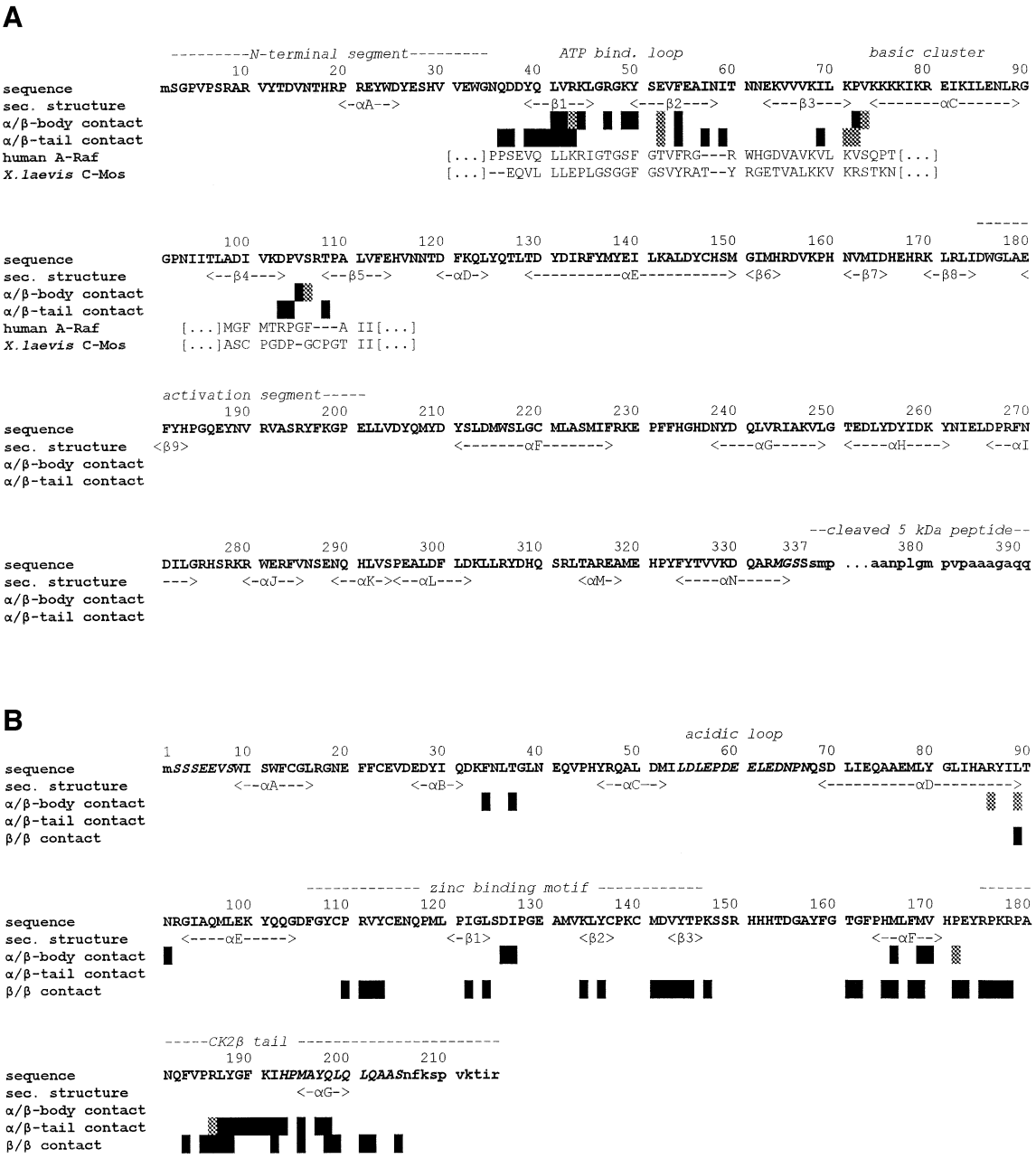

Fig. 1. Sequence overview of human CK2α (**A**) and CK2β (**B**). Small characters in the sequence indicate residues that are truncated or disordered in both copies of the chains and are therefore left out in the final rhCK2α$^{\Delta}$ structure. Positions at which the final $2F_o - F_c$ electron density is badly defined are printed in italics. The contact residues are assigned with black bars. The α/β contacts normally occur twice in the rhCK2$^{\Delta}$ complex; if a certain residue was detected as a contact partner only in one chain it is marked with a grey bar instead of a black one. For human A-Raf and *Xenopus laevis* c-Mos partial sequences are included in (A).

molecular mass of 45.1 kDa. During purification a 5 kDa peptide was spontaneously cleaved from the catalytic subunit leaving a degraded form of ~40 kDa (rhCK2α$^{\Delta}$; Niefind *et al*., 2000), which is around the typical size of CK2α subunits from various sources. The resulting stable CK2 holoenzyme comprising two molecules of rhCK2α$^{\Delta}$ and two molecules of recombinant human CK2β (rhCK2β) is fully active with several typical CK2 substrates (Niefind *et al*., 2000). It is called rhCK2$^{\Delta}$ throughout this paper. Whether this partial degradation of human CK2α occurs also in natural host cells and whether the cleaved peptide has a biological function is not known to date.

Results and discussion

Structure determination

The rhCK2$^{\Delta}$ structure was solved with crystals grown in the presence of Mg^{2+} ions and the non-hydrolysable ATP analogue adenylyl imidodiphosphate (AMPPNP). The crystals belong to space group $P6_3$ with lattice constants $a = b = 176.0$ Å, $c = 93.7$ Å. The asymmetric unit of the

crystals contains one rhCK2$^{\Delta}$ tetramer and has a solvent content of 61%. We hereafter designate the two rhCK2α^{Δ} chains as A1 and A2 and the two rhCK2β chains as B1 and B2.

The crystals were of limited X-ray diffraction quality. The best resolution obtained with a rotating copper anode was 6 Å. At a synchrotron we measured a complete data set to 3.1 Å resolution (Table I), merging data from two crystals. The single diffraction frames showed a significant anisotropy, which was also detected by the program TRUNCATE (CCP4, 1994) for the complete data set. A considerable internal disorder in the crystals was indicated by high mosaicities of the two crystals (1.3 and 1.4°) and an overall *B*-factor of 92.2 Å^2 calculated by TRUNCATE from a Wilson plot.

The structure was solved by a combination of molecular replacement and phase refinement techniques (see Materials and methods) and refined with all reflections from 59.3 to 3.1 Å to a final model with acceptable stereochemical parameters (Table I). A Ramachandran graph for each subunit is shown in Supplementary figure 1, available at *The EMBO Journal* Online.

Table I. Crystallographic analysis

Characteristic data of the rhCK2$^{\Delta}$ synchrotron data set	
Space group	$P6_3$
Lattice constants	$a = b = 176.0$ Å, $c = 93.7$ Å
No. of crystals used	2
Temperature of data collection	100 K
Resolution range	59.3–3.1 Å
No. of observations	268 848
No. of rejections	6073
No. of independent reflections	29 935
Wilson-plot *B*-factor	92.2 Å^2
Multiplicity	8.8
Multiplicity for last shell (3.2–3.1 Å)	6.0
Average of (I/σ_I)	16.7
Average of (I/σ_I) for last shell (3.2–3.1 Å)	2.6
Completeness for whole range	98.4%
Completeness for last shell (3.2–3.1 Å)	90.4%
R_{sym} for whole range	9.6%
R_{sym} for last shell (3.2–3.1 Å)	42.0%
Overview of the final structure model	
Resolution range included in refinement	3.1–60.0 Å
R_{free} (4% of all reflections)[a]	33.8%
R_{work} (96% of all reflections)[a]	26.7%
Real space *R*-value[a]	5.3%
Average *B*-factor	91.0 Å[b]
R.m.s.ds for bonds[a]	0.009 Å
R.m.s.ds for angles[a]	1.5°
Quality of Ramachandran plot	
% residues in most favoured[b] regions	69.5
% residues in additional allowed[b] regions	28.1
% residues in generously allowed[b] regions	2.2
% residues in disallowed[b] regions	0.2
Cross-validated sigmaa estimate of mean coordinate error[a]	1.04 Å
Cross-validated Luzzati estimate of mean coordinate error[a]	0.67 Å

$R_{sym} = \Sigma_h\Sigma_j|I_{h,j} - \langle I_h\rangle|/\Sigma_h\Sigma_j I_{h,j}$, where $I_{h,j}$ is the intensity of the *j*th observation of unique reflection *h*, and $\langle I_h\rangle$ is the mean intensity of that reflection. Reflection intensities related by Friedel symmetric were merged in this data set.
[a]Calculated with CNS (Brünger *et al.*, 1998).
[b]According to PROCHECK (CCP4, 1994).

Quality of the structure

Most parts of rhCK2$^{\Delta}$ are defined by good electron density (see Figure 2 for examples), while in some sections the quality of the density is reduced as indicated by increased real space *R*-factors (Supplementary figure 2). Finally there are regions lacking any ordered electron density. Among these, as indicated in Figure 1, the N-terminus of B2 and the zone Asn206 to Arg215 of B1 and B2 were left out from the final model whereas the zone Asp55 to Asn65 of B1 was modelled as a copy of its equivalent in B2.

Some parts of the chains missing in the initial models, for instance the C- and N-termini of A1 and A2 or the functionally critical zone around Tyr188 of B1 and B2, were added during the refinement process. Model building at 3.1 Å resolution and with model-biased phases is difficult and susceptible to errors. We cannot exclude such errors, which will become apparent with higher-resolution diffraction data, but in view of the final electron densities we are nevertheless confident that we have identified the correct structure from Gly3 to Pro6 of A1 and A2, from Arg333 to Ser337 of A1 and from Pro176 to Gly189 of B1 and B2.

In some other parts (C-terminus of A2, N-terminus and zone Asp55 to Asn65 of B2, zone Phe190 to Ser205 of B1 and B2) the rough trace of the main chain was clear enough, but the conformations of peptide groups and side chains remain questionable. Within such a zone, namely from Met195 to Gln200 of rhCK2β, we modelled an α-helix (αG; Figures 1B and 3D) in agreement with a secondary structure prediction (Korn *et al.*, 1999) and with circular dichroism spectroscopic data, indicating that the CK2 complex formation is accompanied by an increase in the α-helical content of the protomers (Issinger *et al.*, 1992).

Fig. 2. Electron densities in selected regions of rhCK2$^{\Delta}$. All maps apart from that covering the AMPPNP molecule in (D) are sigma-weighted $2F_o - F_c$ electron densities contoured with a 1σ cutoff. The red map in (D) around AMPPNP is an $F_o - F_c$ omit density (4σ cutoff) calculated after a 5000 K simulated annealing run excluding the AMPPNP coordinates. (**A**) Stereo figure of the CK2β tail as part of the β/β contact. The two rhCK2β subunits are distinguished by different colours (red and blue) for the electron densities and the labels. His165 and Met169 of rhCK2β$^{\Delta}$ (Chantalat *et al.*, 1999) and some corresponding water molecules displaced by the formation of the β/β contact are drawn in black. (**B**) Stereo figure of the hydrophobic core of the α/β contact. The colour coding for electron densities and labels is black for the CK2β tail with Tyr188 as the central residue of the whole core, red for the body of the second rhCK2β chain and blue for the participating rhCK2α$^{\Delta}$ subunit. (**C**) The N-terminal segment of rhCK2α$^{\Delta}$ attached to the activation segment (yellow). For comparison the backbone courses of both segments in rmCK2α (Niefind *et al.*, 1999; PDB code: 1DAW) after superimposing on rhCK2α$^{\Delta}$ are drawn in black. Further colour coding for activation segments after three-dimensional fits: red for the partially active CDK2 in complex with a cyclin A fragment (Jeffrey *et al.*, 1995; PDB code: 1FIN) and violet for the inactive CDK2 in isolated form (De Bondt *et al.*, 1993; PDB code: 1HCL). (**D**) Stereo figure of AMPPNP bound to the active site of rhCK2$^{\Delta}$ chain A1. To compare the γ-phosphate positions, AMPPNP as bound to rmCK2α (Niefind *et al.*, 1999) is drawn in black after superimposition of the protein matrices.

In the active site of subunit A1 a bound AMPPNP molecule—but no accompanying Mg^{2+} ions—was detected while A2 was free from a co-substrate analogue. Several peaks of residual electron density were filled with water molecules and phosphate ions in accordance with a phosphate concentration of ~0.2 M in the crystallization

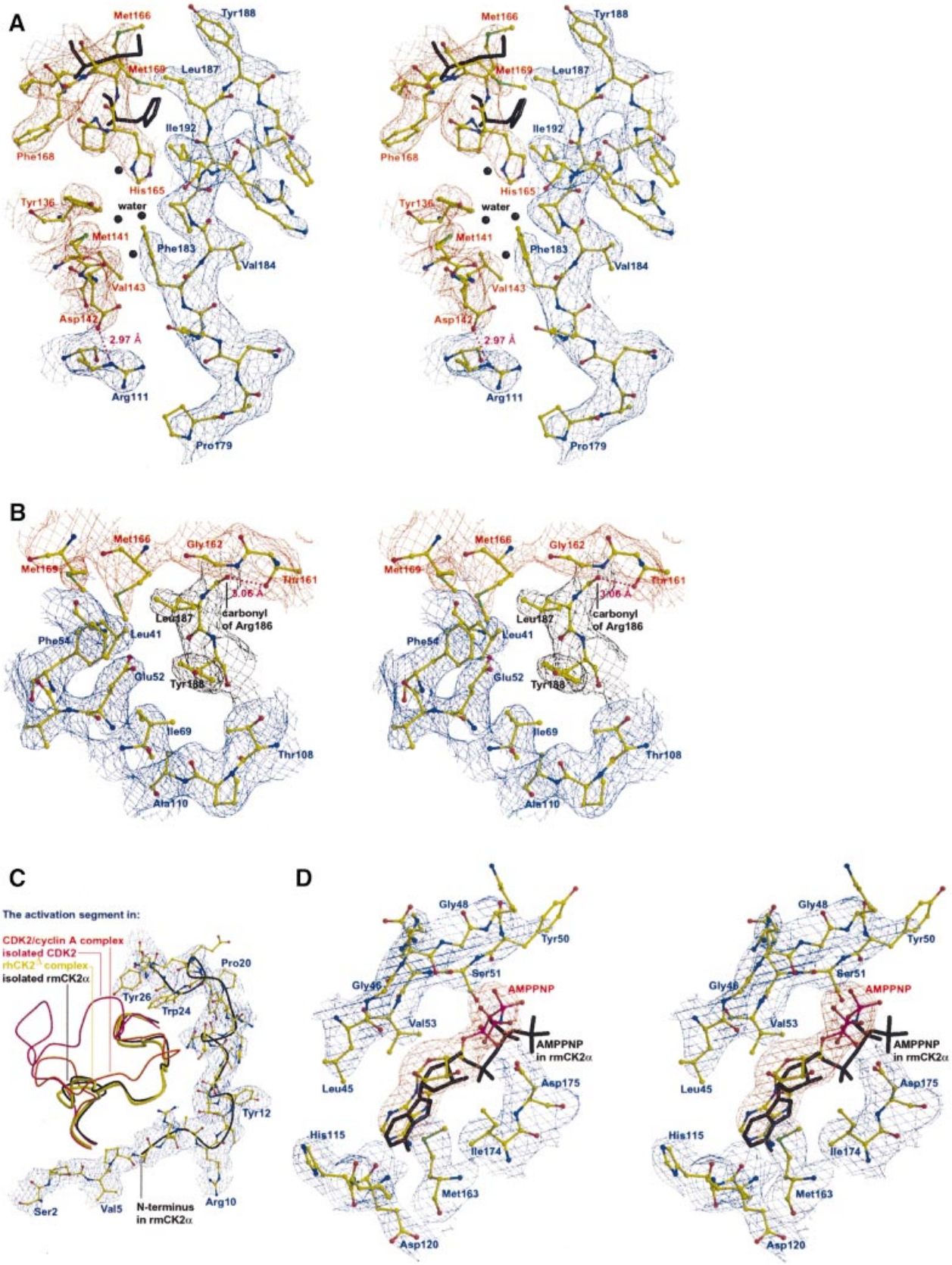

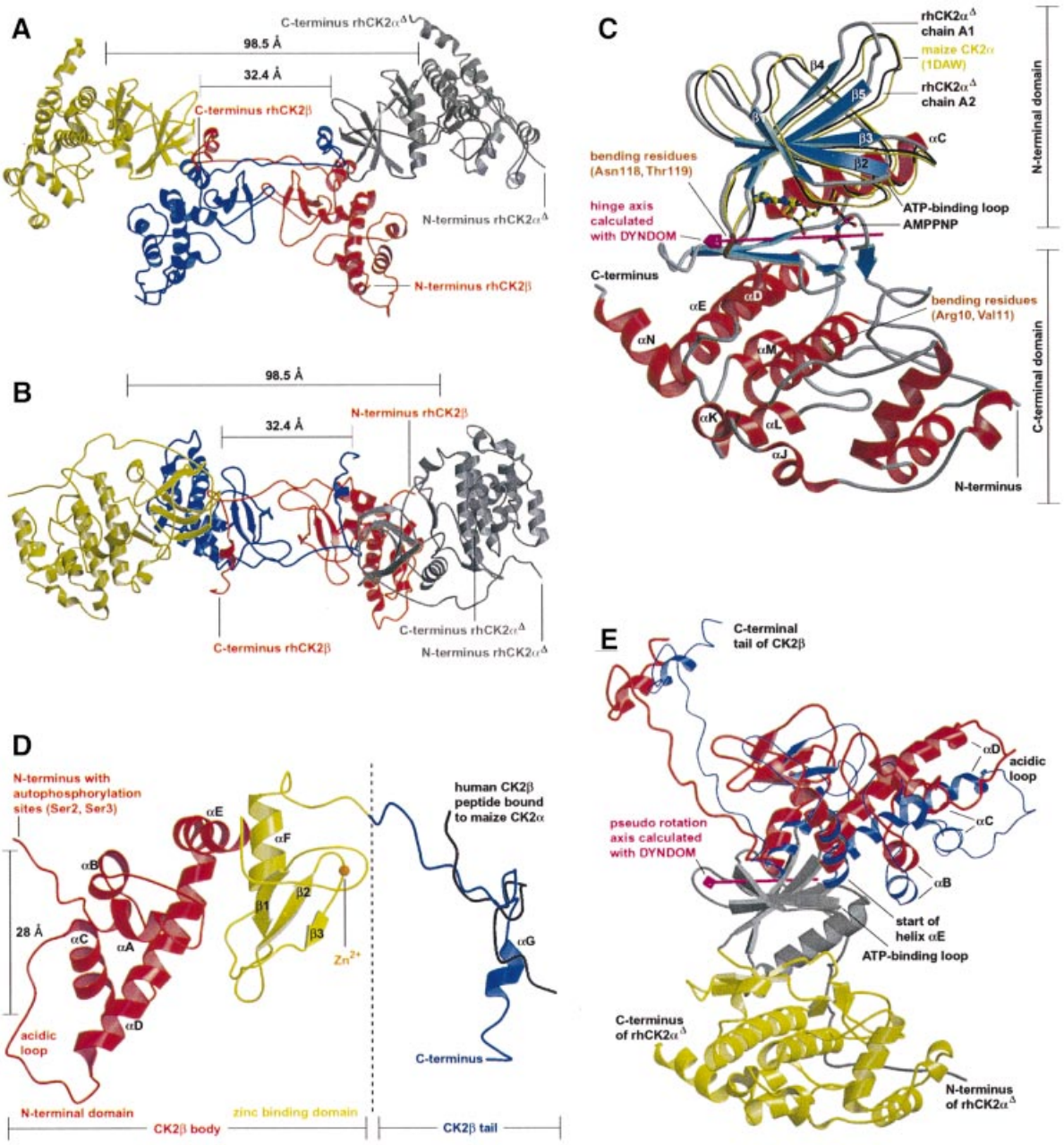

Fig. 3. Various aspects of the rhCK2$^{\Delta}$ structure. (A and B) Overall shape of rhCK2$^{\Delta}$ in a view perpendicular to the local *C*2 axis (**A**) and along this axis (**B**). The two rhCK2β chains are drawn in blue and red, the two rhCK2α$^{\Delta}$ subunits in yellow and grey. (**C**) Structural overview of rhCK2α$^{\Delta}$ chain A1 with bound AMPPNP and interdomain flexibility. The hinge axis and the bending residues of the domain closure motion as detected by DYNDOM (CCP4, 1994) are included. To illustrate the interdomain flexibility, the N-terminal domains of rmCK2α (PDB code: 1DAW) and of rhCK2α$^{\Delta}$ chain A2 are shown in yellow and black, respectively, after three-dimensional alignment of the corresponding C-terminal domains. (**D**) Structural overview of rhCK2β. The human CK2β peptide bound to rmCK2α (black) was taken from PDB file: 1DS5 (Battistutta *et al*., 2000) after superimposition of the corresponding CK2α subunits. (**E**) Intersubunit flexibility at the α/β contact. Subunit A1 is drawn with yellow colour for the C-terminal domain and grey for the N-terminal domain. Subunit B1 bound to A1 by an α/β contact is sketched in red. Subunit B2 is shown in blue after a three-dimensional fit of the N-terminal domain of subunit A2 (not drawn) on that of A1.

drops (Niefind *et al*., 2000). In agreement with rhCK2β$^{\Delta}$ (Chantalat *et al*., 1999) a zinc ion was found in both regulatory subunits.

With 91.0 Å^2 the average *B*-factor of the structure is relatively high, but it corresponds well with the *B*-factor obtained from a Wilson plot (92.2 Å^2; Table I). Furthermore the *R*-factors are relatively large (Table I). While crystal twinning was excluded as a reason, this is likely to be a consequence of the conservative refinement strategy and of the disorder in the crystals, which is indicated by zones of diffuse electron densities and by the drawbacks of the data set mentioned above (low resolution, anisotropy, high mosaicity, high overall *B*-factor).

Overall architecture of rhCK2$^{\Delta}$ and its subunits

Shape of the complex. The rhCK2$^{\Delta}$ complex has the shape of a butterfly in a view from above perpendicular to the molecular 2-fold axis (Figure 3A). Its approximate

dimensions in the directions of the principal axes are 155 × 90 × 66 Å. The second of these axes coincides with the molecular dyad.

Figure 3A and B shows that the central building block of the rhCK2$^{\Delta}$ complex is the rhCK2β dimer bridging the space between both rhCK2α$^{\Delta}$ chains. This happens in such a way that each of the two rhCK2β monomers touches both rhCK2α$^{\Delta}$ subunits, which in contrast make no contact with each other. In fact the centres of mass of the two rhCK2α$^{\Delta}$ molecules are 98.5 Å, their active sites ~80 Å and their nearest atoms 32.4 Å distant from one another (Figure 3A and B).

This central result confirms former findings based on the yeast two-hybrid system (Gietz *et al*., 1995; Boldyreff *et al*., 1996) and is consistent with the monomeric state generally found for isolated CK2α subunits. In contrast it disproves the theoretical CK2 holoenzyme model of Battistutta *et al*. (2000) in which the two catalytic subunits are postulated to be in close contact and the active sites only 13 Å apart from one another.

The shape of rhCK2$^{\Delta}$ in the view of Figure 3B resembles the quaternary structure models that Zhao *et al*. (1998) derived for the holoenzyme of cAMP-dependent protein kinase (CAPK) from neutron small angle scattering experiments. In these models, as in rhCK2$^{\Delta}$, the catalytic C subunits do not touch and have a centre-of-mass distance of as much as 122 Å, while the R_2C_2 complex is formed by the central dimer of two regulatory R subunits. Hence the organization of the rhCK2$^{\Delta}$ complex presented here may also be representative for CAPK and other protein kinases.

Structure of the catalytic subunits. Both rhCK2α$^{\Delta}$ subunits show the typical bilobal architecture of the catalytic core of eukaryotic protein kinases with a β-sheet-rich N-terminal domain, an α-helical C-terminal domain and the active site between them (Figure 3C). Structural superpositions of the two rhCK2α$^{\Delta}$ subunits and of isolated rmCK2α (Niefind *et al*., 1998), including virtually all C_{α} atoms, lead to root mean square deviations (r.m.s.ds) of ~0.8 Å (Table II). These values demonstrate the overall similarity of the superimposed structures, although a closer inspection discloses an interdomain flexibility, which is discussed below.

One of the most conspicuous structural features of rmCK2α, a strong attachment of the N-terminal segment to the activation segment from Asp175 to Glu201 (Niefind *et al*., 1998), is also found in the catalytic subunits of rhCK2$^{\Delta}$ and hence is not affected by rhCK2β (Figure 2C). This observation disproves the hypothesis of Sarno *et al*. (1998) that CK2β and the N-terminal segment of CK2α are competitive for attachment to the activation segment.

The conservation of the activation segment conformation in isolated and complex-bound CK2α is in remarkable contrast to CDK2, where binding of a cyclin A fragment changes the conformation of the activation segment dramatically and brings CDK2 to a partially active conformation (Figure 2C; Jeffrey *et al*., 1995). In this way cyclin A is a molecular switch for CDK2 activity similar to the R-subunit in the case of CAPK. In contrast CK2α is catalytically active both in isolated and in complex-bound form. As an isolated molecule it has a basal activity, but this is elevated for most substrates

Table II. Minimal r.m.s.ds after three-dimensional fits of C_{α} atoms

Catalytic subunits	rhCK2$^{\Delta}$, chain A1[a]	rhCK2$^{\Delta}$, chain A2[a]
rhCK2$^{\Delta}$, chain A1	0.0 Å (337)	0.92 Å (331)
rhCK2$^{\Delta}$, chain A2	0.92 Å (331)	0.0 Å (336)
rmCK2α (1DAW[b])	0.91 Å (327)	0.76 Å (326)
Regulatory subunits	**rhCK2$^{\Delta}$, chain B1[a]**	**rhCK2$^{\Delta}$, chain B2[a]**
rhCK2$^{\Delta}$, chain B1	0.0 Å (200)	0.25 Å (199)
rhCK2$^{\Delta}$, chain B2	0.25 Å (199)	0.0 Å (204)
Isolated CK2β, chain A (1QF8[b])	0.82 Å (165)	0.85 Å (165)
Isolated CK2β, chain B (1QF8[b])	0.67 Å (163)	0.76 Å (163)
Dimers	**rhCK2$^{\Delta}$, CK2β dimer**	
Isolated CK2β, full dimer (1QF8[b])	0.83 Å (328)	

[a]The values in brackets are the numbers of matched C_{α} atoms.
[b]RCSB Protein Data Bank code.

significantly by CK2β, for example, for the synthetic peptide RRDDDSDDD by a factor of four (Boldyreff *et al*., 1994). Calmodulin, however, serves as a much better substrate for CK2α than for the CK2 holoenzyme. More complicated still, these stimulatory and inhibitory effects of CK2β on CK2α strongly depend on the salt concentration and on the presence of effector molecules such as polyamines or polybasic peptides (Pinna and Meggio, 1997). Taken together, CK2β is an environment- and substrate-dependent modulator of CK2α activity rather than an on–off switch (Boldyreff *et al*., 1994). This constitutive activity fully agrees with the structural similarity between isolated and complex-bound CK2α.

Structure of the regulatory subunits. The r.m.s.ds in Table II show that the structure of the CK2β body changes only a little as a consequence of the formation of the rhCK2$^{\Delta}$ complex, and further that the two rhCK2β molecules of the complex are more similar to one another than the two rhCK2α$^{\Delta}$ subunits. This difference is certainly due to the intense interactions between the two rhCK2β chains imposing constraints in favour of structural similarity, whereas the rhCK2α$^{\Delta}$ subunits are not in contact with one another and hence much more free for conformational variations.

Each of the rhCK2β molecules can be divided into a body comprising an α-helical N-terminal domain and a Zn^{2+}-containing domain on the one hand and a C-terminal tail on the other (Figure 3D). While the CK2β body has been characterized by Chantalat *et al*. (1999), the C-terminal tail of CK2β is a new structural element. It points away from the body, forms a 90° knee with a β-hairpin loop with Tyr188 at its top and becomes more and more disordered afterwards (Figure 2A). The importance of this loop is indicated by the fact that the sequence zone R^{186}LYGFKI^{192} is highly conserved. Gly189 and Phe190 are present in all CK2β sequences currently known, while at position 188, apart from tyrosine, phenylalanine also occurs. The CK2β tail has no contact

with the body of its own monomer (Figure 3D) but is stabilized mainly by hydrophobic interactions with the second rhCK2β (Figure 2A) and with one of the rhCK2α$^{\Delta}$ subunits (Figure 2B). These interactions are described below.

The conformation of the CK2β tail is partially consistent with the 3.1 Å resolution structure of rmCK2α in complex with a peptide comprising positions 181–203 of human CK2β (Battistutta *et al*., 2000; PDB code 1DS5). These authors correctly identified the β-hairpin loop (Figure 3D) and its binding site at CK2α. However, the structure of the rmCK2α-bound peptide deviates more from rhCK2$^{\Delta}$ the larger the distances are from the hairpin loop (Figure 3D). This drawback and the absence of any structural overlap with the rhCK2β$^{\Delta}$ structure of Chantalat *et al*. (1999) are certainly the reasons for the wrong architecture of the CK2 holoenzyme model derived by Battistutta *et al*. (2000). This failure demonstrates the limits of a peptide-based approach for the detection of the architecture of an oligomeric protein complex.

Subunit interactions

Overview and designations. The two principal types of protein–protein complexes are homocomplexes between identical subunits, which are usually permanent and evolutionary optimized, and heterocomplexes between non-identical chains, which can be also permanent but are quite often non-obligatory, that is they are made and broken according to the environment and external factors. The size of a protein interface allows an estimation of the permanent or non-obligatory character of a protein–protein contact (Jones and Thornton, 1996).

The rhCK2$^{\Delta}$ complex is a mixture of both complex types. (i) An rhCK2β homodimer formed by an interface that we call 'β/β contact' further on is at the centre of rhCK2$^{\Delta}$ around the molecular 2-fold axis (Figure 3A and B). (ii) There are two 'α/β contacts' between the rhCK2β dimer and either rhCK2α$^{\Delta}$ chain, respectively. Each of these contacts is heterotrimeric, meaning that the interface is composed of one rhCK2α$^{\Delta}$ chain and both rhCK2β subunits (Figure 3A and B). To distinguish the individual contributions we use the designations 'α/β body contact' and 'α/β tail contact' further on. An 'α/β body contact' connects an rhCK2α$^{\Delta}$ subunit and the body of an rhCK2β monomer, while an 'α/β tail contact' connects an rhCK2α$^{\Delta}$ subunit and the tail of an rhCK2β monomer.

The β/β contact. An r.m.s.d. of 0.83 Å between isolated and complex-bound CK2β dimers (Table II) demonstrates that the whole CK2β dimer arrangement is conserved during CK2 complex formation. Consequently the basic principles of the β/β contact in the isolated CK2β dimer (Chantalat *et al*., 1999) are also valid for the CK2β bodies in rhCK2$^{\Delta}$. (i) The interface is formed by the Zn^{2+}-binding motif (Figure 1B). (ii) The interface is mainly hydrophobic with a central area composed of Pro110, Val112, Leu124, Val143 and the hydrophobic parts of Tyr113 and Tyr144. (iii) Well defined intersubunit salt bridges (Arg111 with Asp142; Figure 2A) and hydrogen bonds (Pro110 O with Thr145 N; Val143 O with Val112 N) provide a further stabilization.

Chantalat *et al*. (1999) argue about the fact that the buried surface at the β/β contact in dimers of C-terminally truncated CK2β amounts to only 543 Å^2, which is less than a third of the typical value for protomers of that size (Jones and Thornton, 1996). In rhCK2$^{\Delta}$ this paradox is solved because here the β/β interface, with 1766 Å^2 per subunit, is more than three times as big. The reason for this increase is that in rhCK2$^{\Delta}$ not only the CK2β body contributes to the β/β contact but in an extensive manner so does the tail (Figures 1B and 2A). For example, a novel hydrogen bond is formed from the peptide oxygen of Arg186 in one rhCK2β subunit to the side chain of Thr161 of the other (Figure 2B). And above all in the centre of the new contact region a hydrophobic cluster of Met141, Val143, Tyr136, Phe168, His165 and Met169 from one chain and Phe183, Pro185, Leu187, Ile192 and Met195 from the other forms. Figure 2A illustrates how the side chains of His165 and Met169 change their conformations to participate in this hydrophobic zone and how water molecules found in isolated rhCK2β$^{\Delta}$ dimers (Chantalat *et al*., 1999) are displaced from it. In particular His165 manages in this way to become a member of the aromatic core of the hydrophobic cluster together with Tyr136 and Phe168 from its own and Phe183 from the other subunit (Figure 2A).

The remarkable increase in the β/β contact by the CK2β tail, however, requires a specific conformation of this tail, which also depends—as discussed below—on its participation in the α/β contact and hence on the existence of the complete tetramer. In contrast, for isolated CK2β the region Val170 to Ala180 at the beginning of the tail attenuates the dimerization (Boldyreff *et al*., 1996). This demonstrates the synergistic character of the CK2β tail: it causes aggregation and stability problems in isolated CK2β and was therefore removed for its structure determination (Chantalat *et al*., 1999), but within the CK2 tetramer it stabilizes the β/β and α/β contacts.

The compact nature of the rhCK2β dimer and the extended β/β contact compared with isolated CK2β dimers fully agree with the central role of CK2β dimer formation as the initial step of CK2 holoenzyme assembly (Graham and Litchfield, 2000).

The α/β contacts. The contacts of either catalytic subunit with the CK2β dimer are restricted to the N-terminal lobe of the common core (Figure 1A) typical for all eukaryotic protein kinases (Hanks and Hunter, 1995). More precisely parts of the outer surface of the central β-sheet within the N-terminal domain form the interface with the rhCK2β dimer. Minor contact zones in rhCK2α$^{\Delta}$ are found at strand β3, at the subsequent loop and further at the loop connecting the strands β4 and β5. The main contact region is one of the most important for catalytic activity, namely the strands β1 and β2 and the glycine-rich ATP-binding loop in between (Figure 1A). This fact is especially conspicuous in view of the modulating influence of CK2β on CK2α activity, although it does not allow its detailed structure-based rationalization because the rhCK2$^{\Delta}$ structure presented here contains no substrate molecules.

The observation that no CK2α-specific structural elements but a part of the common protein kinase core forms the α/β interface fits well with the finding that CK2β is able to interact with other protein kinases such as A-Raf (Boldyreff and Issinger, 1997) and c-Mos (Chen *et al*., 1997) as well as with CK2α. These interactions are

activating (A-Raf) (Hagemann *et al*., 1997) or inhibiting (c-Mos) and they are competitive with CK2α so that the same parts of the N-terminal domains are probably involved. Some of the residues in the α/β contact regions including Leu41 or Val42 are conserved between CK2α and A-Raf or c-Mos (Figure 1A), although the fact that CK2β interacts exclusively with A-Raf but not with B-Raf and c-Raf-1 (Hagemann *et al*., 1997) cannot be explained on the primary structure level. In any case the rhCK2$^{\Delta}$ structure supports the view that free CK2β dimers may play a role *in vivo*, interacting with the N-terminal core domains of a certain set of protein kinases leading to specific activations or deactivations.

Such a role of CK2β would require free CK2β dimers in the cell. For a long time CK2 was thought to exist exclusively as a tetrameric complex *in vivo*. Meanwhile, however, several observations indicate that unbound CK2α monomers and CK2β dimers can occur at certain times or in certain compartments (Pinna and Meggio, 1997). Presumably they stem from a spatial or temporal excess of one of the subunits after translation.

Alternatively CK2 holoenzyme could form a pool from which the subunits could be released by dissociation. Generally this possibility is considered improbable because of the spontaneous formation and stable nature of the CK2 tetramers *in vitro* (Pinna and Meggio, 1997). However, some properties of the α/β contact in rhCK2$^{\Delta}$ indicate that an association–dissociation equilibrium *in vivo* should not be completely excluded. (i) Interface size: with an average size of 832 Å^2 the α/β interface is relatively small. Although the precision of this value is reduced at 3.1 Å resolution, it can be compared with the average interface sizes reported by Jones and Thornton (1996), namely 1722 Å^2 for permanent and 804 Å^2 for non-obligate protein–protein complexes. This comparison shows that the α/β contact clearly belongs to the second class. (ii) Intersubunit flexibility: to compare the two α/β contacts of the rhCK2$^{\Delta}$ tetramer we reduced it to two trimers, one of which contained the subunits A1, B1 and B2 and the other the subunits A2, B1 and B2. These trimers were overlayed by superimposing the N-terminal domain of subunit A2 on that of A1 and taking the CK2β dimer along accordingly. This procedure disclosed the flexible character of the α/β contact (Figure 3E). A quantitative analysis of this feature with DYNDOM (CCP4, 1994) revealed a 16.4° pseudo rotation around an axis lying at the outer β-sheet surface of the N-terminal CK2α domain (Figure 3E).

These findings suggest that the CK2 holoenzyme is a transient heterocomplex, which is formed and dissociates *in vivo* for specific functional and regulatory reasons. This idea is speculative at the moment, but if supported by further data in the future it would shed new light on the often addressed problem of regulation of CK2 activity.

Neither the α/β-body nor the α/β-tail contact alone is sufficient to establish a stable α/β interface. However, a value of 491 Å^2 for the α/β-tail contact and only 336 Å^2 for the α/β-body contact demonstrate the major contribution of the α/β-tail contact for the stability of the CK2 holoenzyme, while the α/β-body contact is probably the main determinant for activation. This distinction between activating and stabilizing contacts agrees with the properties of CK2β mutants lacking the C-terminus after Ala180, which retain the capability to activate significantly CK2α but are unable to form stable CK2 holoenzymes (Boldyreff *et al*., 1994).

The cooperativity of the two rhCK2β subunits in rhCK2α$^{\Delta}$ binding can also be seen at an atomic level. At the heart of the contact region a hydrophobic cluster is found that comprises residues from all three contact partners (rhCK2α$^{\Delta}$: Leu41, aliphatic part of Glu52, Phe54, Val67, Ile69, Ala110; first rhCK2β chain: Leu89, Met166, Met169; second rhCK2β chain: Leu187, Tyr188, Ile192). Figure 2B demonstrates the central role of the rhCK2β tail around Tyr188 in this contact zone. After Ile192 both rhCK2β chains are increasingly disordered. They are obviously not important for the holoenzyme formation, fitting the observation that a CK2β mutant lacking the C-terminus after Pro194 behaves biochemically like the wild type (Boldyreff *et al*., 1994).

In contrast to the β/β contact, salt bridges and hydrogen bonds play no important role at the α/β contact region. Unless interface hydrogen bonds are detected in better resolved structures in the future, the absence of specific attachments may be the reason for the inter-subunit mobility at the α/β interface mentioned above (Figure 3E).

Comparison with other protein kinase complex structures. Presently only a limited number of protein kinases have been structurally characterized together with regulatory molecules. Most information exists about cyclin-dependent protein kinases in complex with various cell cycle regulatory proteins: CDK2 was co-crystallized with a cyclin A fragment (Jeffrey *et al*., 1995), with CksHs1 (Bourne *et al*., 1996) and with both a cyclin A fragment and the inhibitory domain of p27^{Kip1} (Russo *et al*., 1996); while for CDK6 complex structures together with the cell cycle inhibitors, p19^{INK4d} (Brotherton *et al*., 1998) and p16^{INK4a} (Russo *et al*., 1998) have been studied. According to these structures the four groups of ligands bind to different regions of the catalytic kinase core: both the cyclins and the INK4 proteins bind to both kinase domains and bridge the active site cleft between them. However, while the cyclins as CDK activators do this in such a way that the activation segment is fixed in an active conformation, it is the other way round with the INK4 proteins. A different inactivation mechanism is found with p27^{Kip1}, which directly blocks the active site of a CDK2–cyclin A complex without inducing major conformational changes in the kinase. Unlike these activators and inhibitors the Cks proteins are targeting molecules. Consequently they bind exclusively to the C-terminal kinase domain far away from the active site cleft.

The α/β contact of rhCK2$^{\Delta}$ represents a valuable new member of the list of interfaces to the catalytic core of protein kinases. To our knowledge the CK2β dimer is the first kinase ligand that binds only to the N-terminal domain. Moreover the α/β contact is restricted to a structurally conserved part of this domain, suggesting that it might represent an interaction site not only used in CK2α.

The fact that CK2β neither blocks the active site nor affects the activation segment agrees with its proposed role as a moderate modulator of CK2α activity rather than an on–off switch. Furthermore, the parallel with the Cks proteins that the interaction site lies completely in one of

the two protein kinase domains suggests that intracellular targeting might be an important function of CK2β, as with the Cks proteins.

Further functional implications

Interdomain and intersubunit flexibility. The CK2β body consists of two domains (Figure 3D) that have a fixed interaction with each other. In contrast in rhCK2α$^{\Delta}$ the two main domains are significantly flexible as illustrated in Figure 3C. A quantitative analysis of this feature with the automatic domain detection program DYNDOM (CCP4, 1994) led to some interesting results. (i) The N-terminal residues Ser2 to Arg10 belong structurally to the C-terminal domain (Figure 3C), which underlines the importance of the attachment between the N-terminal segment and the activation loop. (ii) The 'bending residues' between the two domains are firstly Arg10 to Val11 and secondly Asn118 to Thr119. (iii) The interdomain displacement consists of a rotation of 7.8° around an axis nearly perpendicular to the line connecting the centres of mass of the two domains (Figure 3C). Accordingly DYNDOM regards this rotation as a pure 'closure motion' (Hayward and Berendsen, 1998). (iv) The rotation axis is close to the second zone of bending residues (Figure 3C). Hence, the dipeptide Asn118/Thr119 is classified as an 'effective mechanical hinge' (Hayward and Berendsen, 1998).

From comparisons between protein kinase crystal structures the interdomain mobility within the catalytic core and its importance for the catalytic mechanism are well known (Cox *et al*., 1994). However, we checked all protein kinase entries of the Protein Data Bank and found that rhCK2α$^{\Delta}$ provides the first case in which two significantly different opening states of the active site cleft are seen in the same crystal.

The functional implications of the aforementioned intersubunit flexibility at the α/β interface (Figure 3E) are, however, less clear. One consequence of this mobility is that certain parts of rhCK2β approach the active site of rhCK2α$^{\Delta}$. Examples are helix αB and the unusual 95° knee at the transition from helix αD to αE pointed out already by Chantalat *et al*. (1999) (Figure 3E). Whether this is functionally important and correlated with the conserved character of the amino acids in this region of CK2β remains open at the moment.

Co-substrate binding. Conspicuously, only the active site of chain A1 is occupied by the co-substrate analogue AMPPNP while that of A2 is not. To rationalize this difference we superimposed the two rhCK2α$^{\Delta}$ subunits on each other and on rmCK2α in complex with AMPPNP (Niefind *et al*., 1999) (Figure 3C; Table II). The comparison reveals the unexpected fact that the opening of the active site cleft is distinctly larger in the AMPPNP complexed form of rhCK2α$^{\Delta}$ than in the other, and that in the rmCK2α–AMPPNP complex the cleft is more similar to the empty and less open form of rhCK2α$^{\Delta}$. Obviously not only the opening state of the interdomain crevice but also other, more subtle structural adaptations determine the affinity of the active site for co-substrates.

A comparison of the AMPPNP molecules bound to rmCK2α and to rhCK2$^{\Delta}$ demonstrates that the conformations of the triphosphate regions and the positions of the γ-phosphate groups are very different (Figure 2D). While in rmCK2α the bound AMPPNP is in an active conformation (Niefind *et al*., 1999) this is obviously not the case in rhCK2$^{\Delta}$. A possible reason for this difference is the loss of bound Mg^{2+} ions, which are usually necessary to stabilize the cosubstrate conformation.

The autophosphorylation site. The main autophosphorylation sites of CK2 are Ser2 and Ser3 at the N-terminus of CK2β (Figure 3D). The extent of autophosphorylation is strongly affected by mutations in the acidic loop from Asp55 to Asp64 (Boldyreff *et al*., 1994), supporting the notion that in unphosphorylated CK2 the N-terminus of CK2β is attached to the acidic loop and that this contact is broken by autophosphorylation. The rhCK2$^{\Delta}$ structure neither shows such a contact nor does it rule out this hypothesis: although the acidic loop and the N-terminus of rhCK2β are >25 Å apart from one another (Figure 3D), large *B*-factors in both elements indicate a high flexibility, making conformations plausible in which they are attached to one another.

There has been speculation that autophosphorylation of CK2 may be a potential regulatory mechanism for the enyzme. However, according to Bodenbach *et al*. (1994) the consequences of autophosphorylation for the kinetic parameters are negligible. This observation is confirmed by the rhCK2$^{\Delta}$ structure, which shows that the distance from the autophosphorylation site to the nearest active site is >40 Å.

The acidic loop. The acidic loop (Asp55–Asp64) as part of an extended acidic groove (Figure 4) plays an important role in the modulation of CK2 activity. Essentially this loop down-regulates the activity of the enzyme, but neutralization or shielding of its negative charge by mutation of the negative residues to alanine (Boldyreff *et al*., 1994), by addition of polylysine or by increasing the ionic strength, hyperactivates CK2. The negatively charged character of this loop is well conserved as is the basic cluster $K^{74}KKKIKR^{80}$ within the αC region of CK2α (Figure 1A), which is the potential binding site for the acidic determinants of CK2 substrates and for the strong inhibitor heparin. An interaction between these two regions within the CK2 holoenzyme was the first direct α/β contact to be postulated (Lozeman *et al*., 1990).

This idea was supported by crosslinking and immunoprecipitation experiments (Krehan *et al*., 1996), but biochemical and mutagenesis investigations (Boldyreff *et al*., 1993) suggested a more complex picture. According to these studies CK2β can protect CK2α partially against inhibition by heparin. This protection is much less effective with CK2β mutants in which the negative charges of the acidic loop are removed, supporting the notion that heparin and the acidic loop of CK2β compete for binding to the basic cluster of CK2α in agreement with the hypothesis outlined above. Additionally, however, Boldyreff *et al*. (1993) have shown that a hyperactivating CK2β mutant with a neutralized acidic loop still retains the full potential to form a stable CK2 holoenzyme. Hence the ability of the acidic loop to down-regulate the activity of CK2 is not coupled to its integration in the α/β interface. This conclusion is supported by the rhCK2$^{\Delta}$

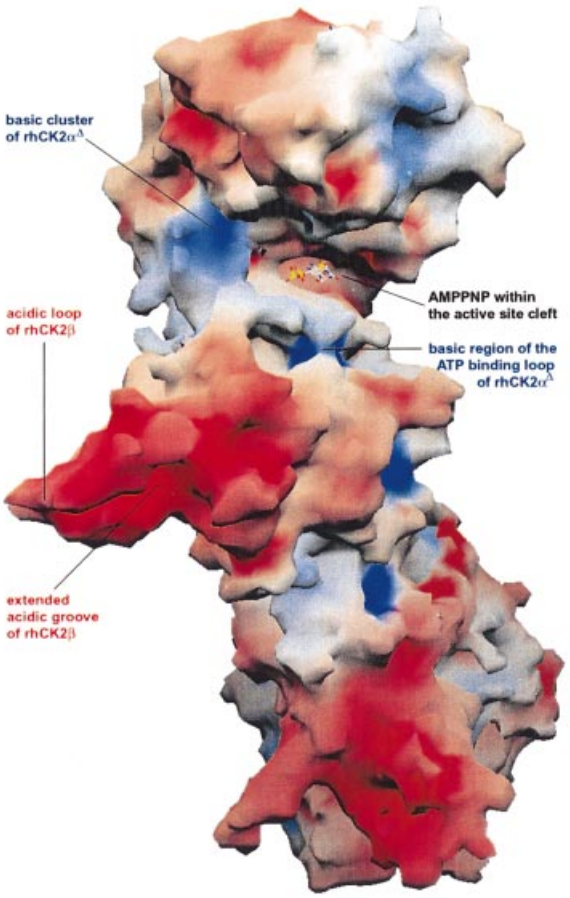

Fig. 4. Electrostatic surface of rhCK2$^{\Delta}$. The surface is coloured according to the electrostatic potential ranging from deep blue (positive charge) to red (negative charge). Atomic charges were assigned by GRASP (Nicholls *et al*., 1991) using default values.

structure showing that the acidic loop of rhCK2β is >30 Å distant from the nearest basic cluster of rhCK2α$^{\Delta}$.

If not by a direct attachment within the holoenzyme, how else does the acidic loop affect the activity of CK2? The electrostatic surface shown in Figure 4 illustrates the strong differences in the charge distribution at the outer surface of the rhCK2$^{\Delta}$ complex. In particular the interior of the active site cleft is highly positive, not only because of the basic cluster but also from the R^{43}KLGRGK^{49} motif of the ATP binding loop. In contrast the acidic CK2β loop forms a negatively charged, prominent wedge at one of the borders of the cleft. This charge distribution suggests two ideas: (i) the acidic loop might disturb the access of negatively charged substrates to the active site, or (ii) the interaction between the acidic loop and the basic cluster might involve subunits from different complexes, by plugging the negatively charged wedge of one CK2 complex into a positive active site cleft of a second one. The latter idea would be consistent with the propensity of CK2 to form higher-order aggregates (Glover, 1986).

Both these hypotheses are speculative at the moment. Structures of CK2 complexes including substrate molecules or heparin would be helpful to obtain further insights into the functional roles both of the acidic loop and of the basic cluster.

Materials and methods

Production and crystallization of rhCK2$^{\Delta}$

rhCK2$^{\Delta}$ was prepared and crystallized as described by Niefind *et al*. (2000). Briefly, optimal crystals grew at 12°C by vapour diffusion in sitting drops in which 3 µl of an rhCK2$^{\Delta}$ preparation with 5.0 mg/ml protein in 25 mM Tris–HCl, 300 mM NaCl, 1 mM dithiothreitol pH 8.5, had been mixed with 3 µl of 2.0 mM $MgCl_2$, 3 µl of 1 mM AMPPNP, 1 µl of 10% (w/v) polyethylene glycol (PEG) 400 dodecylether and 1.5 µl of reservoir solution composed of 20% (w/v) PEG 3350, 200 mM K_2HPO_4 pH 9.3.

X-ray diffraction data collection

X-ray diffraction data were collected at the EMBL beamline BW7b at DESY, Hamburg, using a MAR345 imaging plate detector. For the diffraction experiments a cryo-protectant solution containing 25% (w/v) PEG 3350, 25% (v/v) glycerin, 0.2 M K_2HPO_4, 0.1% (w/v) PEG 400 dodecylether was added in small portions to the crystallization drops until the resulting mixture was a suitable cryo buffer for the crystals.

The diffraction data (Table I) were collected from two crystals and processed with the HKL package (Otwinowski and Minor, 1997), followed by TRUNCATE (CCP4, 1994) to obtain structure-factor amplitudes. The processed data set was checked for merohedral twinning with CNS (Brünger *et al*., 1998) but no indications of it could be detected.

Structure determination and refinement

The structure was determined by molecular replacement in combination with phase refinement techniques. Various search models for cross rotation and translation searches were extracted from the coordinates of rmCK2α (Niefind *et al*., 1999) and rhCK2β$^{\Delta}$ (Chantalat *et al*., 1999).

Numerous molecular replacement searches were performed with AMoRe (CCP4, 1994) and CNS (Brünger *et al*., 1998) at various resolutions. A significant solution was detected only with a poly-alanine backbone of rmCK2α as search model and the locked [non-crystallographic symmetry (NCS) constrained] rotation option of AMoRe for the cross rotation step.

As we were unable to find a molecular replacement solution for CK2β we started the refinement of the structure on the basis of the rhCK2α$^{\Delta}$ sub-structure. All subsequent refinement and density modification calculations were performed with CNS (Brünger *et al*., 1998) while model building was performed with program O (Jones *et al*., 1991).

To locate the CK2β subunits, the initial phases based on the rhCK2α$^{\Delta}$ sub-structure alone were refined by NCS averaging and solvent flattening. In this way an improved electron density was achieved in which a long α-helix could be found in a region not occupied by the rhCK2α$^{\Delta}$ sub-structure. This helix was correctly interpreted as helix αD of rhCK2β (Figure 3D) and served as a starting point for the final insertion of the complete molecule.

As it was impossible to apply the NCS operations of the rhCK2α$^{\Delta}$ sub-structure to the growing model of the rhCK2β subunit, we located the second rhCK2β chain independently of the first one, calculated the NCS matrix for the rhCK2β sub-structure approximately and refined the NCS mappings for both sub-structures on the electron density level using DM (CCP4, 1994).

The refinement was governed strictly by following the R_{free} value (Brünger, 1992). Strong NCS restraints for atomic coordinates and *B*-factors were applied. Individual temperature factors were refined after a CNS run with the script 'optimize_rweight.inp' (Brünger *et al*., 1998) had provided a suitable weighting factor to lower R_{free} significantly. During model building the coordinates of rmCK2α (Niefind *et al*., 1998) and rhCK2β$^{\Delta}$ (Chantalat *et al*., 1999) were used as matrices as far as possible.

In retrospect we confirmed the orientation and position of CK2β relative to CK2α using the refined rhCK2β monomers as search models in molecular replacement searches with CNS (Brünger *et al*., 1998).

Structure interpretation and documentation

We used some CCP4 programs (CCP4, 1994) for structure interpretation and documentation purposes: PROCHECK to validate the refined complex, AREAIMOL to calculate solvent-accessible surfaces and

DYNDOM to detect domains and hinge axes. R.m.s.ds (Table II) were calculated with the least-squares-fit options of O (Jones *et al*., 1991).

Figures 2 and 3 were prepared with BOBSCRIPT (Esnouf, 1997) and Raster3D (Merritt and Bacon, 1997) and Figure 4 with GRASP (Nicholls *et al*., 1991). The coordinates and the structure factors have been deposited at the RCSB Protein Data Bank (ID code 1JWH).

Supplementary data

Supplementary data for this paper are available at *The EMBO Journal* Online.

Acknowledgements

We would like to dedicate the elucidation of the structure of protein kinase CK2 holoenzyme to Professor Ed Krebs for his pioneering work in the field of protein kinase research. The generous support by Professor Dietmar Schomburg, Cologne, and the excellent assistence by Dr Paul Tucker at the EMBL outstation in Hamburg during data collection are gratefully acknowledged. We thank Professor Jonathan Howard, Cologne, for carefully reading the manuscript. K.N. obtained an EMBO short-term fellowship (ASTF9305). I.E. is funded by the Professor-Dr-Werner-Petersen-Stiftung, Kiel, Germany. O.-G.I. is supported by the Danish Cancer Society (grant No. 96 100 40) and the Danish Research Council (grant No. 9601695).

References

Battistutta,R., Sarno,S., De Moliner,E., Marin,O., Issinger,O.-G., Zanotti,G. and Pinna,L.A. (2000) The crystal structure of the complex of *Zea mays* α subunit with a fragment of human β subunit provides the clue to the architecture of protein kinase CK2 holoenzyme. *Eur. J. Biochem.*, **267**, 5184–5190.

Bodenbach,L., Fauss,J., Robitzki,A., Krehan,A., Lorenz,P., Lozeman, F.J. and Pyerin,W. (1994) Recombinant human casein kinase II. A study with the complete set of subunits (α, α′ and β), site-directed autophosphorylation mutants and a bicistronically expressed holoenzyme. *Eur. J. Biochem.*, **220**, 263–273.

Boldyreff,B. and Issinger,O.-G. (1997) A-Raf kinase is a new interacting partner of protein kinase CK2β subunit. *FEBS Lett.*, **403**, 197–199.

Boldyreff,B., Meggio,F., Pinna,L.A. and Issinger,O.-G. (1993) Reconstitution of normal and hyperactivated forms of casein kinase-2 by variably mutated β-subunits. *Biochemistry*, **32**, 12672–12677.

Boldyreff,B., Meggio,F., Pinna,L.A. and Issinger,O.-G. (1994) Protein kinase CK2 structure–function relationship: effects of the β subunit on reconstitution and activity. *Cell. Mol. Biol. Res.*, **40**, 391–399.

Boldyreff,B., Mietens,U. and Issinger,O.-G. (1996) Structure of protein kinase CK2: dimerization of the human β-subunit. *FEBS Lett.*, **379**, 153–156.

Bourne,Y., Watson,M.H., Hickey,M.J., Holmes,W., Rocque,W., Reed, S.I. and Tainer,J.A. (1996) Crystal structure and mutational analysis of the human CDK2 kinase complex with cell cycle-regulatory protein CksHs1. *Cell*, **84**, 863–874.

Brotherton,D.H. *et al*. (1998) Crystal structure of the complex of the cyclin D-dependent kinase Cdk6 bound to the cell cycle inhibitor $p19^{INK4d}$. *Nature*, **395**, 244–250.

Brünger,A.T. (1992) The free *R* value: a novel statistical quantity for assessing the accuracy of crystal structures. *Nature*, **335**, 472–475.

Brünger,A.T. *et al*. (1998) Crystallography and NMR system (CNS): a new software system for macromolecular structure determination. *Acta Crystallogr. D*, **54**, 905–921.

Chantalat,L., Leroy,D., Filhol,O., Nueda,A., Benitez,M.J., Chambaz, E.M., Cochet,C. and Dideberg,O. (1999) Crystal structure of the human protein kinase CK2 regulatory subunit reveals its zinc finger-mediated dimerization. *EMBO J.*, **18**, 2930–2940.

Chardot,T., Shen,H. and Meunier,J.-C. (1995) Dual specificity of casein kinase II from the yeast *Yarrowia lipolytica*. *C. R. Acad. Sci. III*, **318**, 937–942.

Chen,M., Li,D., Krebs,E.G. and Cooper,J.A. (1997) The casein kinase 2 β subunit binds to Mos and inhibits Mos activity. *Mol. Cell. Biol.*, **17**, 1904–1912.

Chester,N., Yu,I.J. and Marshak,D.R. (1995) Identification and characterization of protein kinase CK2 isoforms in HeLa cells. *J. Biol. Chem.*, **270**, 7501–7514.

Collaborative Computational Project No. 4 (1994) The CCP4 suite: programs for protein crystallography. *Acta Crystallogr. D*, **50**, 760–763.

Cox,S., Radzio-Andzelm,E. and Taylor,S.S. (1994) Domain movements in protein kinases. *Curr. Opin. Struct. Biol.*, **4**, 893–901.

De Bondt,H.L., Rosenblatt,J., Jancarik,J., Jones,H.D., Morgan,D.O. and Kim,S.-H. (1993) Crystal structure of cyclin-dependent kinase 2. *Nature*, **363**, 595–602.

Esnouf,R.M. (1997) An extensively modified version of MolScript that includes greatly enhanced coloring capabilities. *J. Mol. Graph.*, **15**, 132–134.

Gatica,M., Hinrichs,M.V., Jedlicki,A., Allende,C.C. and Allende,J.E. (1993) Effect of metal ions on the activity of casein kinase II from *Xenopus laevis*. *FEBS Lett.*, **315**, 173–177.

Gietz,R.D., Graham,K.C. and Litchfield,D.W. (1995) Interactions between the subunits of casein kinase II. *J. Biol. Chem.*, **270**, 13017–13021.

Glover,C.V.C. (1986) A filamentous form of *Drosophila* casein kinase II. *J. Biol. Chem.*, **261**, 14349–14354.

Graham,K.C. and Litchfield,D.W. (2000) The regulatory β subunit of protein kinase CK2 mediates formation of tetrameric CK2 complexes. *J. Biol. Chem.*, **275**, 5003–5010.

Guerra,B., and Issinger,O.-G. (1999) Protein kinase CK2 and its role in cellular proliferation, development and pathology. *Electrophoresis*, **20**, 391–408.

Hagemann,C., Kalmes,A., Wixler,V., Schuster,T. and Rapp,U.R. (1997) The regulatory subunit of protein kinase CK2 is a specific A-Raf activator. *FEBS Lett.*, **403**, 200–202.

Hanks,S.K. and Hunter,T. (1995) Protein kinases 6. The eukaryotic protein kinase superfamily: kinase (catalytic) domain structure and classification. *FASEB J.*, **9**, 576–596.

Hayward,S. and Berendsen,H.J.C. (1998) Systematic analysis of domain motions in proteins from conformational change. New results on citrate synthase and T4 lysozyme. *Proteins*, **30**, 144–154.

Issinger,O.-G., Brockel,C., Boldyreff,B. and Pelton,J.T. (1992) Characterization of the α and β subunits of casein kinase 2 by far-UV CD spectroscopy. *Biochemistry*, **31**, 6098–6103.

Jeffrey,P.D., Russo,A.A., Polyak,K., Gibbs,E., Hurwitz,J., Massague,J. and Pavletich,N.P. (1995) Mechanism of CDK activation revealed by the structure of a cyclinA–CDK2 complex. *Nature*, **376**, 313–320.

Jones,S. and Thornton,J.M. (1996) Principles of protein–protein interactions. *Proc. Natl Acad. Sci. USA*, **93**, 13–20.

Jones,T.A., Zou,J.-Y., Cowan,S.W. and Kjeldgaard,M. (1991) Improved methods for building protein models in electron density maps and the location of errors in these models. *Acta Crystallogr. A*, **47**, 110–119.

Korn,I., Gutkind,S., Srinivasan,N., Blundell,T.L., Allende,C.C. and Allende,J.E. (1999) Interactions of protein kinase CK2 subunits. *Mol. Cell. Biochem.*, **191**, 75–83.

Krehan,A., Lorenz,P., Plana-Coll,M. and Pyerin,W. (1996) Interaction sites between catalytic and regulatory subunits in human protein kinase CK2 holoenzyme as indicated by chemical cross-linking and immunological investigations. *Biochemistry*, **35**, 4966–4975.

Lozeman,F.J., Litchfield,D.W., Piening,C., Takio,K., Walsh,K.A. and Krebs,E.G. (1990) Isolation and characterization of human cDNA clones encoding the α and the α′ subunits of casein kinase II. *Biochemistry*, **29**, 8436–8447.

Marin,O., Meggio,F., Sarno,S., Cesaro,L., Pagano,M.A. and Pinna,L.A. (1999) Tyrosine versus serine/threonine phosphorylation by protein kinase casein kinase-2. *J. Biol. Chem.*, **274**, 29260–29265.

Merritt,E.A. and Bacon,D.J. (1997) Raster3D: photorealistic molecular graphics. *Methods Enzymol.*, **277**, 505–524.

Nicholls,A., Sharp,K. and Honig,B. (1991) Protein folding and association: insights from the interfacial and thermodynamic properties of hydrocarbons. *Proteins*, **11**, 281–296.

Niefind,K., Guerra,B., Pinna,L.A., Issinger,O.-G. and Schomburg,D. (1998) Crystal structure of the catalytic subunit of protein kinase CK2 from *Zea mays* at 2.1 Å resolution. *EMBO J.*, **17**, 2451–2462.

Niefind,K., Pütter,M., Guerra,B., Issinger,O.-G. and Schomburg,D. (1999) GTP plus water mimics ATP in the active site of protein kinase CK2. *Nature Struct. Biol.*, **6**, 1100–1103.

Niefind,K., Guerra,B., Ermakowa,I. and Issinger,O.-G. (2000) Crystallization and preliminary characterization of crystals of human protein kinase CK2. *Acta Crystallogr. D*, **56**, 1680–1684.

Otwinowski,Z. and Minor,W. (1997) Processing of X-ray diffraction data collected in oscillation mode. *Methods Enzymol.*, **276**, 307–326.

Padmanabha,R., Chen-Wu,J.L., Hanna,D.E. and Glover,C.V. (1990) Isolation, sequencing and disruption of the yeast *CKA2* gene: casein

kinase II is essential for viability in *Saccharomyces cerevisiae*. *Mol. Cell. Biol.*, **10**, 4089–4099.

Pinna,L.A. and Meggio,F. (1997) Protein kinase CK2 ('casein kinase-2') and its implication in cell division and proliferation. *Prog. Cell Cycle Res.*, **3**, 77–97.

Russo,A.A., Jeffrey,P.D., Patten,A.K., Massagué,J. and Pavletich,N.P. (1996) Crystal structure of the $p27^{Kip1}$ cyclin-dependent-kinase inhibitor bound to the cyclin A–Cdk2 complex. *Nature*, **382**, 325–331.

Russo,A.A., Tong,L., Lee,J.-O., Jeffrey,P.D. and Pavletich,N.P. (1998) Structural basis for inhibition of the cyclin-dependent kinase Cdk6 by the tumor suppressor $p16^{INK4a}$. *Nature*, **395**, 237–243.

Sarno,S., Marin,O., Ghisellini,P., Meggio,F. and Pinna,L.A. (1998) Biochemical evidence that the N-terminal segments of the α subunit and the β subunit play interchangeable roles in the activation of protein kinase CK2. *FEBS Lett.*, **441**, 29–33.

Seldin,D.C. and Leder,P. (1995) Casein kinase 2α transgene-induced murine lymphoma: relation to Theileriosis in cattle. *Science*, **267**, 894–897.

Wilson,L.K., Dhillon,N., Thorner,J. and Martin,G.S. (1997) Casein kinase II catalyses tyrosine phosphorylation of the yeast nucleolar immunophilin Fpr3. *J. Biol. Chem.*, **272**, 12961–12967.

Zhao,J., Hoye,E., Boylan,S., Walsh,D.A. and Trewhella,J. (1998) Quaternary structures of a catalytic subunit–regulatory subunit dimeric complex and the holoenzyme of the cAMP-dependent protein kinase by neutron contrast variation. *J. Biol. Chem.*, **273**, 30448–30459.

Received March 30, 2001; revised July 6, 2001; accepted August 3, 2001